Fırat Üniversitesi Deneysel ve Hesaplamalı Mühendislik Dergisi

FUJECE

Klasik Dikdörtgen Büzülmeli Savakların Mansabında Oluşan Yerel Oyulmaların HAD Yöntemi Kullanılarak İncelenmesi

Erdinc İKİNCİOGULLARİ [1*], Muhammet Emin EMİROĞLU [2], Mehmet Cihan AYDİN [3]

[1]İnşaat Mühendisliği Bölümü, Mühendislik Fakültesi, Bingöl Üniversitesi, Bingöl, Türkiye.
[1]Enerji, Çevre ve Doğal Afet Araştırmaları Merkezi, Bingöl Üniversitesi, Bingöl, Türkiye.
[2]İnşaat Mühendisliği Bölümü, Mühendislik Fakültesi, Fırat Üniversitesi, Elâzığ, Türkiye.
[3]İnşaat Mühendisliği Bölümü, Mühendislik Fakültesi, Bitlis Eren Üniversitesi, Bitlis, Türkiye.
[1]eikinciogullari@bingol.edu.tr, [2]memiroglu@firat.edu.tr, [3]mcaydin@gmail.com

Geliş Tarihi: 16.10.2025
Kabul Tarihi: 01.12.2025
Düzeltme Tarihi: 23.11.2025
doi: https://doi.org/10.62520/fujece.1804990
Araştırma Makalesi

Alıntı: E. İkincioğulları, M. E. Emiroğlu ve M. C. Aydın,'' Klasik dikdörtgen büzülmeli savakların mansabında oluşan yerel oyulmaların HAD yöntemi kullanılarak incelenmesi", Fırat Üni. Deny. ve Hes. Müh. Derg., vol. 5, no 1, pp. 231-249, Şubat 2026.

Özet

Hidrolik yapıların güvenliği sosyal, ekonomik ve çevresel öneme sahiptir. Yerel oyulmanın neden olduğu hasarları ortadan kaldırmak için ya oyulma tamamen önlenmeli ya da oyulma derinliği en aza indirilmelidir. Bu çalışmada, serbest düşülü klasik büzülmeli dikdörtgen savakların mansabında oluşan yerel oyulma sayısal olarak incelenmiştir. Sayısal analizlerde Flow3D yazılımı ve k-ε türbülans modelleri kullanılmıştır. Maksimum oyulma derinliğini belirlemek için analizler üç birim debi (q=0.15, 0.30 ve 0.60 m^3/s m) ve üç düşü yüksekliği (H=0.25, 0.50 ve 1.00 m) için gerçekleştirilmiştir. Ayrıca, su jeti hızı ve çarpma açısı incelenmiştir. Tüm durumlar için denge oyulma derinliğinin yaklaşık %90'ına ilk 15–20 dakika içinde ulaşıldığı ve bunun önceki çalışmalarla uyumlu olduğu belirlenmiştir. Sonuçlara göre, birim debinin artmasıyla denge oyulma derinliği yaklaşık 0.16 m'den 0.23 m'ye yükselmektedir. Ancak, düşü yüksekliğinin belirli bir değerin üzerine çıkmasıyla, mansap havuzuna daha fazla hava kabarcığı girmesine bağlı olarak oyulma derinliği üzerindeki etkinin bir miktar azaldığı görülmüştür. Hesaplanan jet çarpma hızları yaklaşık 2.0 ile 4.9 m/s arasında değişmekte, çarpma açısı ise düşü yüksekliğinin artmasıyla birlikte yaklaşık 82°'ye kadar çıkmaktadır. Sayısal modelden elde edilen sonuçların genel olarak deneysel çalışmalarla uyumlu olduğu tespit edilmiştir. Bu çalışma, serbest düşülü koşullarda yüksek düşülü savakların mansabında oluşan yerel oyulmanın üç boyutlu HAD tabanlı değerlendirmesini sunması ve uzun dönem denge oyulma derinliği ile jet çarpma karakteristiklerinin pratik olarak tahmin edilmesine yönelik bir yaklaşım önermesi bakımından özgün niteliktedir.

Anahtar kelimeler: Yerel oyulma, Oyulma süreci, Serbest düşülü savaklar, Baraj güvenliği, Havza morfolojisi, Flow3D®, Hesaplamalı akışkanlar dinamiği (HAD)

*Yazışılan yazar

İntihal Kontrol: Evet – Turnitin
Şikayet: fujece@firat.edu.tr

Firat University Journal of Experimental and Computational Engineering

Investigation of Local Scour at Classical Contracted Rectangular Weir Downstream using CFD

Erdinc IKINCIOGULLARI[1,*], Muhammet Emin EMIROGLU[2], Mehmet Cihan AYDIN[3]

[1]Civil Engineering Department, Bingol University, Bingol, Türkiye.
[1]Center For Energy, Environment, and Natural Disaster, Bingol University, Bingol, Türkiye.
[2]Civil Engineering Department, Firat University, Elazig, Türkiye.
[3]Civil Engineering Department, Bitlis Eren University, Bitlis, Türkiye.
[1]eikinciogullari@bingol.edu.tr, [2]memiroglu@firat.edu.tr, [3]mcaydin@gmail.com

Received: 16.10.2025
Accepted: 01.12.2025
Revision: 23.11.2025
doi: https://doi.org/10.62520/fujece.1804990
Research Article

Citation: E. İkincioğulları, M. E. Emiroğlu and M. C. Aydın, "Investigation of local scour at classical contracted rectangular weir downstream using CFD", Firat Univ. Jour.of Exper. and Comp. Eng., vol. 5, no 1, pp. 231-249, February 2026.

Abstract

The safety of hydraulic structures has social, economic, and environmental significance. To eliminate the damage induced by local scouring, either the scouring should be prevented entirely or the scouring depth should be minimized. This study numerically investigated the local scour that develops in the plunge pool downstream of high-head, classical contracted rectangular weirs operating under free overfall conditions. In the numerical analysis, a three-dimensional Reynolds-averaged Navier–Stokes (RANS) model with a standard k–ε turbulence closure was implemented in Flow-3D®. The analyses were conducted for three unit flow rates (q=0.15, 0.30, and 0.60 m^3/s m) and three drop heights (H=0.25, 0.50, and 1.00 m) to determine the maximum scouring depth. Furthermore, the water jet velocity and impingement angle were analyzed. The experimental results were utilized to test the accuracy of the numerical model. For all cases, about 90 % of the equilibrium scour depth was reached within the first 15–20 min, consistent with previous studies. According to the results, the equilibrium scour depth increased from approximately 0.16 m to 0.23 m when the unit discharge was raised. However, after a specific value of the head height, the effect on the depth of scouring is slightly reduced due to the increased air entrainment entering the downstream pool. Computed jet impact velocities ranged from about 2.0 to 4.9 m/s, with impact angles increasing up to ~82° as the drop height increased. The results of the numerical model are generally compatible with experimental studies. This study is original in that it provides a three-dimensional CFD-based assessment of local scour downstream of high-head weirs under free overfall conditions and proposes a practical approach to estimate long-term equilibrium scour depth and jet impact characteristics.

Keywords: Local scour, Scour process, Free overfall, Dam safety, Basin morphology, Flow3D®, CFD

*Corresponging author

1. Introduction

Energy demand increases rapidly due to population and economic growth. Along with the energy demand in the 21st century, many high-head dams have been built. However, due to the increase in the drop height of the dam, local scouring in the downstream pool may damage the hydraulic structure or cause its destruction. Thus, the accurate prediction of local scouring that may occur in the hydraulic structure downstream is essential. Although scouring has attracted the attention of researchers, few studies address scouring the downstream of free-falling weirs in literature. For instance, Stein and Julien [1] conducted experimental research to determine the correlations between scour depth, sediment concentration, scour-hole volume, and time for a free overfall weir. Ghodsian et al. [2] conducted an experimental study about local scour. They established the effect of tailwater depth on the scour hole and the height of the dunes. A rigorous parametric examination of scour depth downstream of a steep vertical drop in uniform sediments was conducted experimentally by Dey and Raikar [3]. The results of the experimental study were utilized to demonstrate how several factors, including temporal variation, affected equilibrium scour depth. Ghodsian et al. [4] researched to more thoroughly examine the impact of critical characteristics, including sediment gradation, on the scour parameters caused by free-falling jets.

In recent years, Computational Fluid Dynamics (CFD) techniques in hydraulics have become popular in research, besides conventional experimental studies. Validated and tested CFD software is a powerful tool that is employed to simulate complicated fluid flow problems, and it could save time and costs in hydraulic model studies. The multi-phase and turbulent flows that include liquids, gases, and solid particles, such as scour problems downstream of a dam, require the solution of complex equations for fluid motion. These numerical methods have improved significantly over time and have been employed by several researchers. In their initial study, Olsen and Melaaen [5] successfully applied three-dimensional numerical models to calculate local scour around a cylindrical bridge pier. Lin and Falconer [6] developed a numerical model in estuarine and coastal waters for three-dimensional suspended sediment. The authors tested the model against analytical solutions and experimental data for different flow types and boundary conditions. Richardson and Panchang [7] studied the local scouring around a bridge pier using Flow3D® software and the RNG k-ε turbulence model. The authors utilized a three-dimensional computational model to determine the complex flow field for flatbed and equilibrium scour conditions. They found that the three-dimensional model simulated the complex flow fields around the bridge pier. Later, other researchers such as Wu et al. [8], Yafei Jia et al. [9], Liu et al. [10], Vasquez and Walsh [11], Abbasi et al. [12], Castillo and Carrillo [13], Epely-Chauvin et al. [14], Cihan et al. [15], Pang et al. [16], Pourshahbaz et al. [17], Man et al. [18], Aydin et al. [19], Ikinciogullari et al. [20], Kumar and Afzal [21], and Wang et al. [22] successfully employed various CFD techniques and software to investigate hydraulic scour problems numerically. Cihan et al. [15] provided a general framework for using CFD in hydraulic structures. Aydın and Karaduman [23] and Aydin et al. [19] numerically modelled the experimental models developed by Dey and Sarkar [24] and Dey and Raikar [3] with Flow 3D software. They obtained good results with CFD simulations for scour in specific downstream hydraulic structures compared to experimental findings. Yan et al. [25] studied a sediment-scour model using OpenFOAM software and the conformal moving-mesh technique. They stated that the agreement of the model was proven to be a valid tool for simulating local scour issues caused by submerged wall jets by experimental and computational findings.

Contracted rectangular weirs are widely used in hydraulic engineering. However, these numerical studies provided valuable insights into scour mechanisms but generally did not address free-overfall conditions downstream of high-head classical contracted rectangular weirs, nor did they quantify jet impact characteristics and scour geometry over a wide range of unit discharges and drop heights. Therefore, there remains a research gap regarding the three-dimensional CFD modelling of local scour in plunge pools downstream of free-overfall contracted rectangular weirs.

The free overfall from high-head weirs could lead to significant scouring at the downstream of hydraulic structures such as dams. This local scour could seriously compromise the safety of hydraulic structures over time. Therefore, it is of vital importance to identify local scouring in advance. The aim of this study

is to numerically investigate the local scour that develops downstream of free-overfall classical contracted rectangular weirs and to assess the ability of a three-dimensional Flow-3D software to reproduce experimentally observed scour characteristics. The originality of the present study lies in the three-dimensional CFD modelling of local scour in the plunge pool downstream of free-overfall classical contracted rectangular weirs. Based on a combined experimental–numerical dataset for nine test conditions encompassing three unit discharges and three drop heights, the study systematically evaluated the influence of discharge and head on equilibrium scour depth, scour-hole geometry, and jet impact characteristics. Furthermore, the temporal evolution of scour depth was represented by an exponential function and used to extrapolate short-term simulations (up to about 1 h) to 9 h equilibrium conditions, providing a practical procedure to reduce computational cost in scour analyses.

2. Methodology

Figure 1 demonstrates a schematic representation of the definition sketch and the scour of a free overfall on the weir. The scouring properties of the water jet, which was designed as a free overfall with a contracted weir, are presented in Figure 1, where x_1 and x_2 refer to the distances between the point of the maximum scour and downstream and upstream of the bed level, respectively. x_m is the distance between the weir wall and the maximum scour point, x_3 refers to the distance between the maximum scour point and the maximum accumulation point (Δx), x_b is used to describe the distance between the dune's center and the weir. d refers to the scour point in any x value, and d_s refers to the maximum scour.

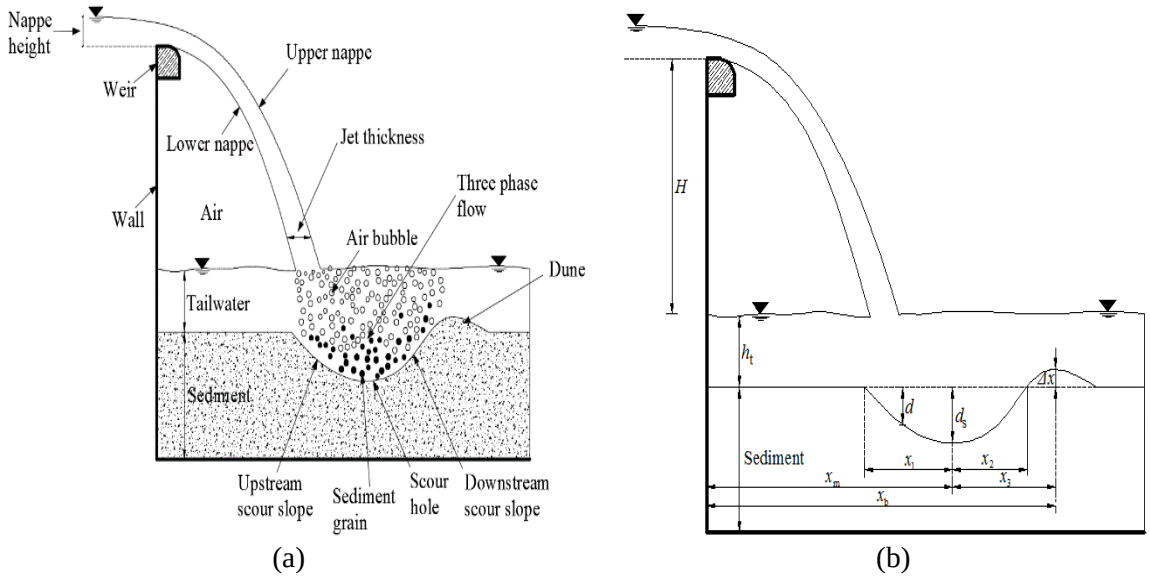

Figure 1. (a) Sketch of a scour phenomenon definition; (b) The properties of the scour sketch

2.1. Experimental setup

The scour experiments employed for comparison purposes were conducted under the experimental setup in Firat University Hydraulic Laboratory, as presented in Figure 2. Three pumps were operated using two tanks of 50 and 100 m^3 in the laboratory, each pumping approximately 77 L/s of discharge from the 100 m^3 tank to the 50 m^3 tank 11 m above. By using the spillway on the 50 m^3 tank, the water level is maintained at a static level. Water was taken from a 50 m^3 tank located 8 m above the laboratory ground level for the experiments. The plunging pool width was 1.25 m, height was 2 m, and length was 2.50 m. The upstream channel was 0.51 m wide, 0.85 m high, and 6.00 m long. A 1.00 m uniform sand layer was placed on the plunging pool. The bed material included uniform sediment with a median size of 2 mm.

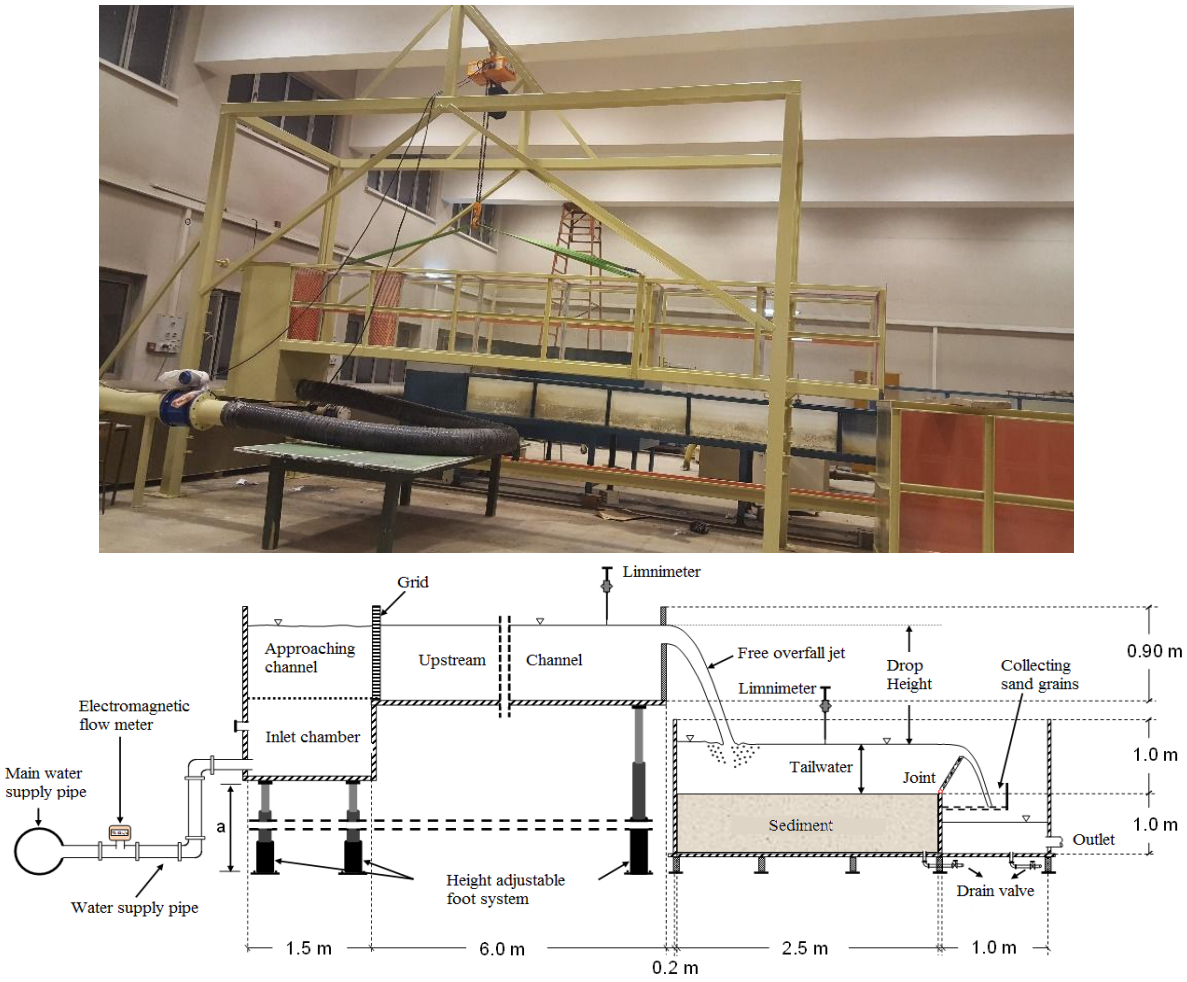

Figure 2. Experimental setup (Reprinted from authors previous study [30])

Nine analyses were conducted in the study for a tailwater depth (0.25 m), three unit discharges (0.15, 0.30, and 0.60 m^3/s m), and three drop heights (for 0.25, 0.50, and 1.00 m). The classical contracted rectangular weir was 0.25 m high, 0.167 m wide, with 0.05 m material wall thickness (see Figure 3a). A suppressed weir is shown in Fig. 3(b).

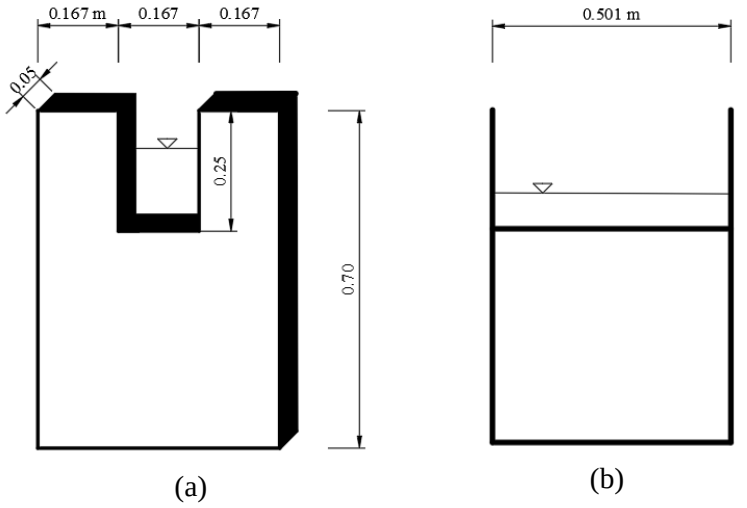

Figure 3. Geometry of the weir: (a) Contracted weir; (b) Suppressed weir

2.2. Numerical model

The three-dimensional numerical analyses were conducted with Flow3D® software. In numerical analysis, the standard k–ε turbulence model was preferred because it provides a reasonable compromise between numerical stability, computational cost, and accuracy for high-Reynolds-number, fully turbulent, free-surface jets and scour flows, and has been successfully applied in previous CFD studies of local scour [20,26–29]. The theoretical details for the numerical solutions are summarized as follows:

2.2.1. Flow governing equations

CFD is significant for solving several hydraulic engineering problems due to the advances in computer technology. This method provides solutions based on simple equations, such as the Navier-Stokes and continuity equations in the flow-motion calculation. This technique provides fast results since it can analyze several hydraulic parameters simultaneously. One of the most complicated problems in hydraulics is turbulent free surface flow in numerical modelling.

Navier-Stokes equations are the basic equations in fluid mechanics that define the motion of incompressible fluid flow. RANS (Reynolds Averaged Navier-Stokes) equations could be written in the Cartesian coordinate system for a three-dimensional flow as follows:

$$\frac{\partial u_i}{\partial x_i} = 0 \tag{1}$$

$$\frac{\partial u_i}{\partial t} + u_j \frac{\partial u_i}{\partial x_j} = -\frac{1}{\rho}\frac{\partial p}{\partial x_i} + \frac{\partial}{\partial x_i}\left(\upsilon \frac{\partial u_i}{\partial x_j} - \overline{u_i' u_j'}\right) + S_i \tag{2}$$

In which p is the pressure, u is the velocity, ρ is the mass density of water, t is the time, $\overline{u_i' u_j'}$ is the Reynolds stress, S_i is the source term, and ν is the kinematic viscosity of water. The k-ε turbulence closure model has been utilized for simulations.

2.2.2. Sediment model

In the numerical model, several methods were employed for sediment transport and scour models in the literature. According to Soulsby and Whitehouse [31], the critical Shields coefficient could be calculated with Eq. (3).

$$\theta_{cr,i} = \frac{0.3}{1+1.2d_{*,i}} + 0.055\left[1 - \exp(-0.02d_{*,i})\right] \tag{3}$$

where $d_{*,i}$ is a dimensionless parameter calculated with Eq. (4).

$$d_{*,i} = d_i \left[\frac{\rho(\rho_s - \rho)\|g\|}{\mu^2}\right]^{1/3} \tag{4}$$

where, d_i refers to the grain diameter, ρ_s refers to the specific mass of sediment, $\|g\|$ refers to the gravity magnitude, and μ refers to the dynamic viscosity. The following equation was used for calculating the local bed shear stress:

$$\theta_i = \frac{\tau}{\|g\| d_i(\rho_i - \rho)} \tag{5}$$

Shields coefficient was updated for inclined surfaces as reflected in Eq. (6).

$$\theta'_{cr,i} = \theta_{cr,i} \frac{\cos\psi \sin\beta + \sqrt{\cos^2\beta \tan^2\varphi_i - \sin^2\psi \sin^2\beta}}{\tan\varphi_i} \tag{6}$$

Where φ_i is the angle of repose (default 32°), β represents the bed slope, and ψ denotes the angle between the flow and the upslope direction for flow directly up to a slope, ψ=0°. Equation 7 was used by Mastbergen and Van Der Berg [32] to determine the speed of lifting at which the silt was seen.

$$u_L = \alpha_i n_s {d_{*,i}}^{0.3} (\theta_i - {\theta'}_{cr,i})^{1.5} \sqrt{\frac{\|g\| d_i (\rho_s - \rho)}{\rho}} \tag{7}$$

where, α_i is the entrainment coefficient and n_s is the outward-pointing normal to the packed bed interface.

The settling velocity equation proposed by Soulsby and Whitehouse [31] was employed:

$$u_s = \frac{\upsilon}{d_i}\left[(10.36^2 + 1.049 {d_{*,i}}^3)^{0.5} - 10.36\right] \tag{8}$$

Bed-load transport refers to the mechanism of sediment conveyance characterized by the rolling or bouncing of particles along the surface of a packed sediment bed. Meyer-Peter and Müller [33] suggested Eq. (9) for the dimensionless bed movement ratio (ϕ_i).

$$\phi_i = \beta_{MPM} (\theta_i - {\theta'}_{cr,i})^{1.5} \tag{9}$$

where β_{MPM} can be adjusted based on the bed motion. There will be no bed movement if this value is set to zero. It might be raised to allow for further bed mobility (default value is 8).

ϕ_i refers to the dimensionless bed-load transport rate and is associated with the volumetric bed-load transport rate, $q_{b,i}$ [34].

$$q_{b,i} = \phi_i \left[\|g\| \frac{(\rho_s - \rho_f)}{\rho_f} {d_i}^3\right]^{1/2} \tag{10}$$

Flow3D® allows changes in sediment model coefficients to verify numerical studies with experimental data. In the current study, three validation coefficients were employed for three drop heights. In these analyses, three model parameters known to influence scour depth, namely the entrainment coefficient, the bed roughness/d_{50} ratio, and the bed load coefficient, were employed as calibration parameters. The calibration coefficients that minimized the relative error are summarized in Table 1.

Table 1. Calibration coefficients used for different drop heights

Drop Height (m)	Entrainment coefficient (–)	Bed roughness/d_{50} ratio (–)	Bed load coefficient (–)
0.25	0.0005	0.80	3
0.50	0.0005	0.40	3
1.00	0.0005	0.05	1

3. Results and Discussion

In the numerical model, several studies were performed largely to ascertain the influence of cell size on the solution. In the first stage, the cell size was fixed at 0.04 m and analyses were conducted for approximately 900 seconds. Then, the cell size was reduced to 0.03 m and the analyses were conducted for 900-1800 seconds. Finally, to determine whether the scour depth reached a steady state, the cell size was reduced to 0.02 m and analyses were conducted for 1800-2400 seconds. It was observed that the scour depth did not change (Fig. 4). Thus, it was concluded that it would be sufficient to continue the analysis with a cell size of 0.03 m for the mesh block employed in the drop pool (Fig. 5a, block 1). As seen in Fig. 4, the solutions acquired stability with these three mesh structures, which decreased sequentially. Therefore, the sensitivity of the simulation results to the mesh structure was minimized, and the final mesh structure was determined.

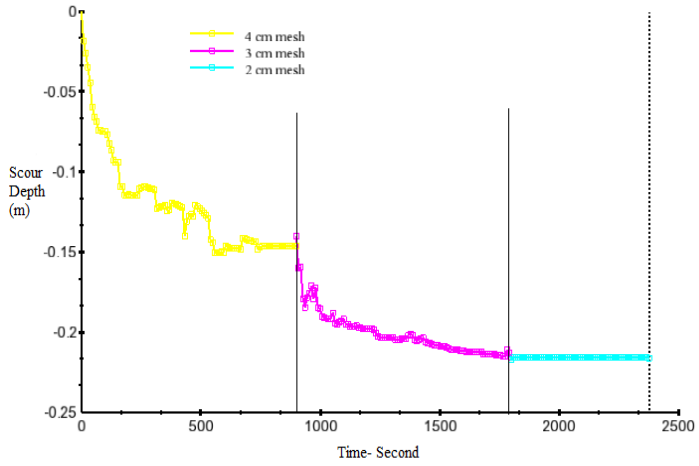

Figure 4. The testing of mesh quality (Reprinted from authors previous study [20])

Mesh dimensions should not be determined as small enough to extend the solution time unnecessarily or large enough to obtain inaccurate results. As a result of the preliminary analysis, it was concluded that a uniform mesh with a size of 0.03 m was suitable for the first and the second blocks out of the three blocks. The dimension of the third block located at the upstream channel was determined as 0.06 m since it did not affect the scouring depth (Fig. 5a). Then, the symmetry (*S*) boundary condition was selected to ensure the transition between the blocks, the discharge (*Q*) boundary condition was selected for the channel upstream, and the pressure (*P*) boundary condition was defined downstream of the channel to allow the tailwater effect. Then, the wall (*W*) boundary condition was selected for channel edges (Fig. 5b).

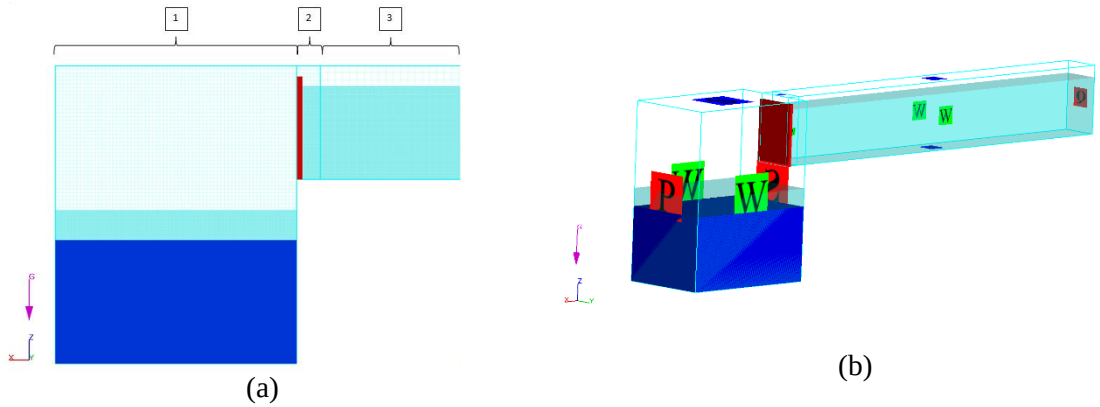

Figure 5. (a) Design of mesh blocks; **(b)** determination of boundary conditions

The simulation outputs for the numerical analysis conducted with Flow3D® software for various unit discharge values are presented in Fig. 6. As mentioned above, it was observed that scouring increased rapidly within the first 15-20 minutes, then continued to increase gradually and reached the equilibrium scouring depth. However, due to the increased momentum with the increase in discharge, the time required to reach the equilibrium scour depth also increased.

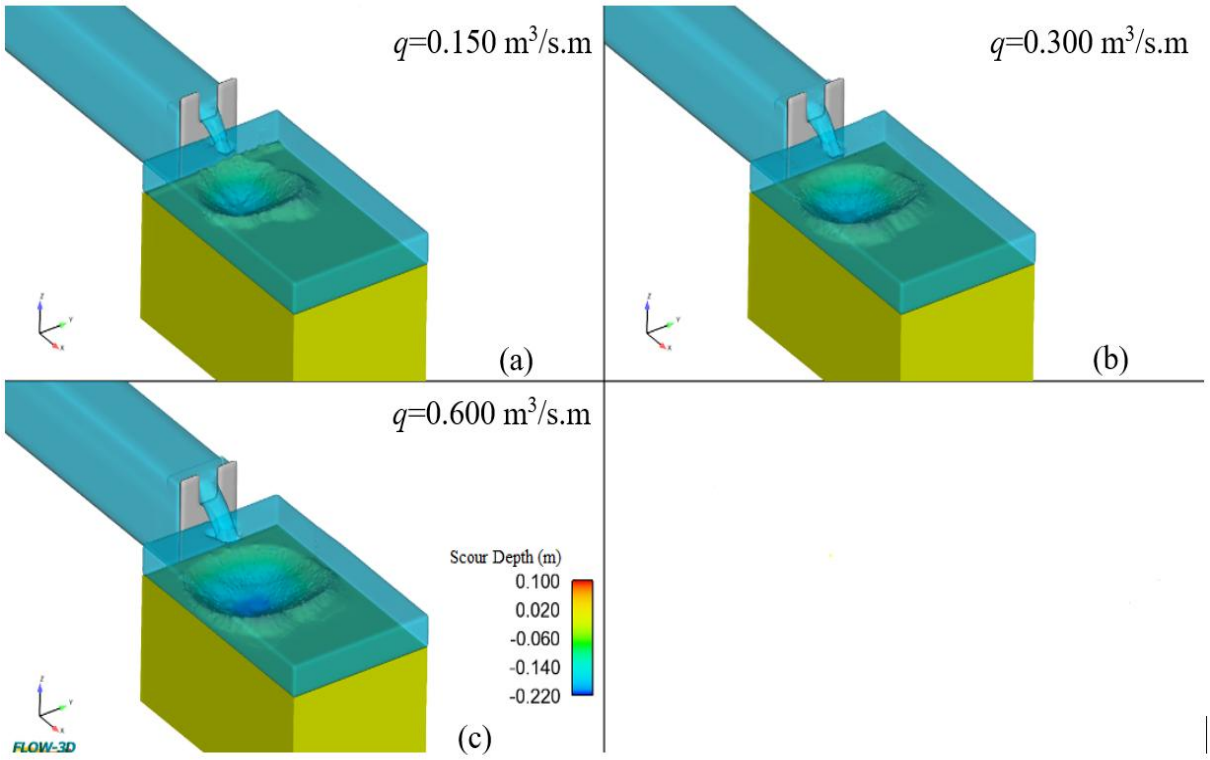

Figure 6. Equilibrium scour depths: a) for q= 0.150 m^3/s m, H=0.25 m and h_t=0.25 m, b) for q=0.300 m^3/s m, H=0.25 m and h_t=0.25 m and c) for q=0.600 m^3/s m, H=0.25 m and h_t=0.25 m

The physical experiments [30] were conducted for 9 hours. Numerical analysis for nine hours could take weeks, especially for scouring problems. For that reason, the numerical studies were continued for approximately 2500-4000 seconds and then were plotted as exponential functions to estimate the results after 9 hours in this study. The present results confirm that approximately 90% of the equilibrium scour depth develops within the first 15–20 min, which is consistent with the experimental observations of Dey and Raikar [3] and with the numerical findings of Fan et al. [35] and Liu et al. [36], who also reported rapid scour development and early equilibrium times. This rapid development is thought to occur due to the high initial momentum of the plunging jet and the relatively fine, uniform sediment that allows fast particle entrainment. Dey and Raikar [3] conducted 9-hour experiments for equilibrium scour depth, but they reached the equilibrium depth within almost 600 seconds. Fan et al. [35] observed that in their simulation, the equilibrium depth was attained in 60 minutes, and 90% of the equilibrium scouring depth was attained in the first 20 minutes. Liu et al. [36] reported that the equilibrium scour depth obtained after 60 minutes was close to the experimental results.

Figure 7 shows the results of the numerical solution of the scour depth for different times for q=0.150 m^3/s m, H=0.50 m, and h_t=0.25 m. When the 1-hour numerical finding was compared with the 9-hour experimental result, the 1-hour numerical result corresponded to approximately 90 percent of the 9-hour experimental result.

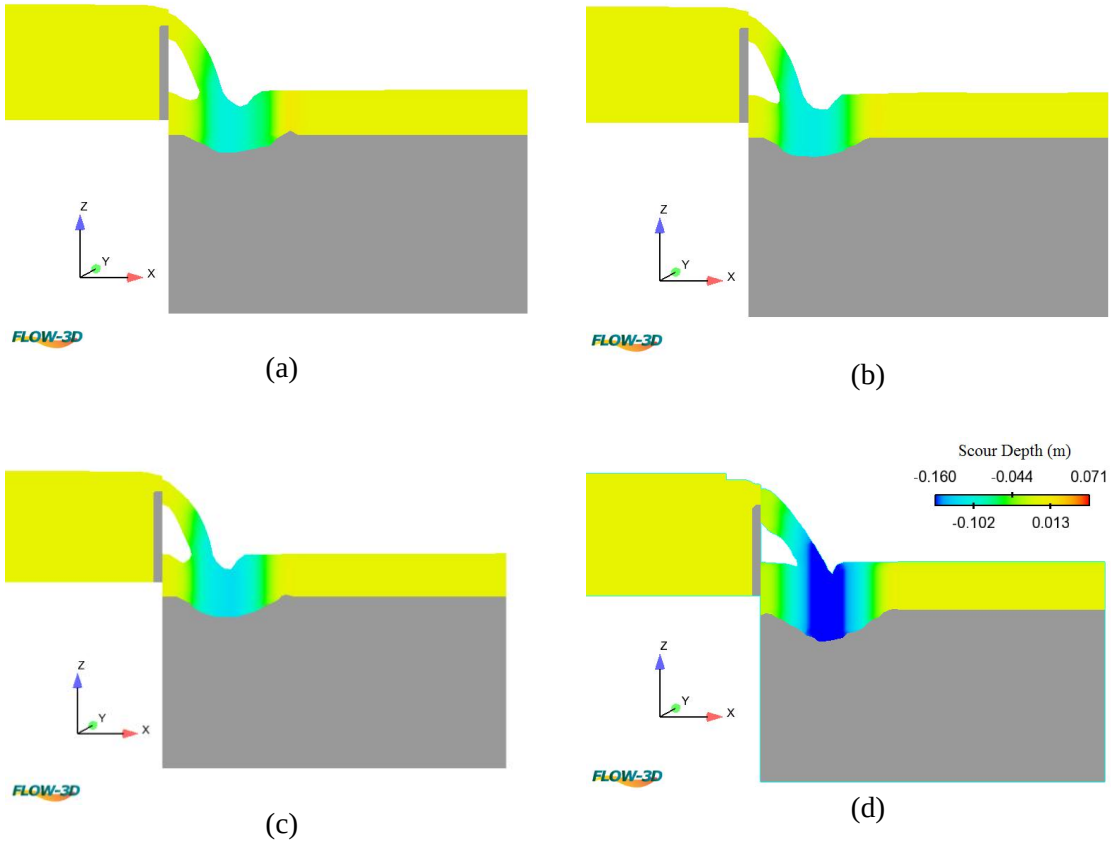

Figure 7. Scour depth longitudinal section for H=0.50 m, q=0.150 m^3/s m, and h_t=0.25 m by CFD: a) for 900 s, b) for 1800 s, c) for 2700 s, and d) for 3600 s

The scour graph changes with the exponential function. The equation for the exponential function, fitted to the results obtained with numerical studies, is presented in Eq. (11).

$$d = a \cdot (1 - exp(-b \cdot t)) \tag{11}$$

where d refers to the scour depth, t refers to the scour time (second), a and b refer to the exponential function coefficients. These coefficients and the determination coefficient obtained with the equations are presented in Table 2. The graphs of the curves fitted to Eq. (11) demonstrate that the determination coefficient (R^2) varied between 0.72-0.96 (Fig. 8).

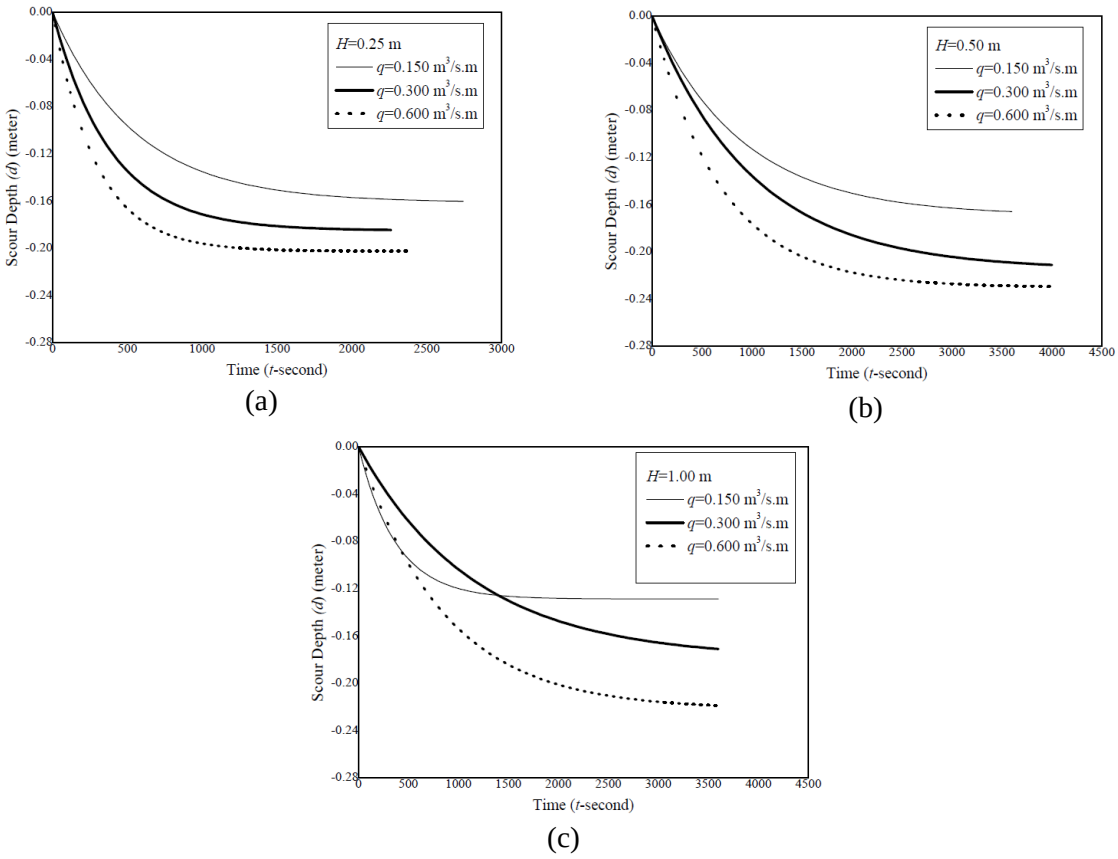

Figure 8. Temporal variations in maximum scour depth: a) for *H*=0.25 m; b) for *H*=0.50 m and c) for *H*=1.00 m

Table 2. Constants in Eq. 11

Analyse No	*a*	*b*	R^2
AN-1	-0.16150	0.00182	0.92
AN-2	-0.18528	0.00260	0.96
AN-3	-0.20280	0.00344	0.90
AN-4	-0.16939	0.00110	0.72
AN-5	-0.21534	0.00099	0.81
AN-6	-0.23037	0.00145	0.75
AN-7	-0.12901	0.00267	0.92
AN-8	-0.17918	0.00087	0.83
AN-9	-0.22242	0.00118	0.88

The experimental results for 9 hours, the numerical results for 1 hour, and scour depths estimated with an exponential function for 9 hours are presented in Table 3. The results of both studies showed that an increase in the unit discharge caused the scour depth to rise. The scour depth increased in both studies by increasing the drop height from 0.25 m to 0.50 m. This significant increase is considered to result from the increase in jet momentum and impact velocity acting on the movable bed. However, when the drop height was increased from 0.50 m to 1.00 m, there was no significant change in the experimental results due to the increased air bubbles that entered the water jet. At the same time, a slight decrease was recorded in the numerical results. This situation was also consistent with the experimental findings of Baylar and Emiroglu [37]. They experimentally investigated the air entrainment rate in sharp-crested, broad-crested, and labyrinth weirs as a function of discharge and drop height. The authors found that when discharge and drop height increased, there was a considerable rise in the amount of air bubble entrainment into the flow. It was found that when the discharge and drop height increased, the tendency for air bubble entrainment into the flow also tended to rise [37]. The relative error rates for the scour

values obtained with experimental and numerical studies are presented in Table 3. The experimental scour depth (d_{s_e}) was compared with the 9-hour scour depth (d_{s_9}) to determine the relative error ε using Eq. (12). The review of these values suggested that the maximum relative error was around 18%. These error rates were likely acceptable for the investigated scour problems, where the experimental and numerical findings were consistent.

$$\varepsilon = \left|\frac{d_{s\_e} - d_{s\_9}}{d_{s\_e}}\right| \cdot 100 \tag{12}$$

where d_{s_e} is the experimental scour depth after 9 hours and d_{s_9} is the estimated scour depth after 9 hours. In Table 3, d_{s_1} is the scour depth after 1 hour determined using CFD.

Table 3. Experimental and numerical equilibrium scour depths comparison at the classical contracted rectangular weir downstream

Model No	**Experiment No**	q	H	h_t	**Experimental Results** [30]	d_{s_1}	d_{s_9}	ε
		(m^3/sm)	(m)	(m)	d_{s_e} (m)	(m)	(m)	(%)
AN-1	1	0.150	0.25	0.25	0.154	0.165	0.162	5.2
AN-2	2	0.300	0.25	0.25	0.182	0.185	0.185	1.6
AN-3	4	0.600	0.25	0.25	0.232	0.216	0.203	12.5
AN-4	5	0.150	0.50	0.25	0.177	0.182	0.169	4.5
AN-5	6	0.300	0.50	0.25	0.182	0.212	0.215	18.1
AN-6	8	0.600	0.50	0.25	0.216	0.242	0.230	6.5
AN-7	9	0.150	1.00	0.25	0.146	0.139	0.129	11.6
AN-8	10	0.300	1.00	0.25	0.174	0.193	0.179	2.9
AN-9	12	0.600	1.00	0.25	0.216	0.233	0.222	2.8

The horizontal (V_x) and vertical (V_z) water jet velocities, the impact velocity of the water jet on the downstream pool (V_j), and the angle of jet impact (ζ) are presented in Table 4. It was noted that the water jet impact velocity typically increased due to the increasing momentum with the rise in unit discharge. However, when the unit discharge is kept constant and the drop height is increased, the impact velocity and the impact angle of the water jet increase due to the transformation of the potential energy of the water jet into kinetic energy. In general, the increase in unit discharge leads to a decrease in the angle of impact of the water jet. However, due to the increased momentum, there would be a decrease in the angle of the water jet, which would hit a farther point in the downstream channel (Fig. 9).

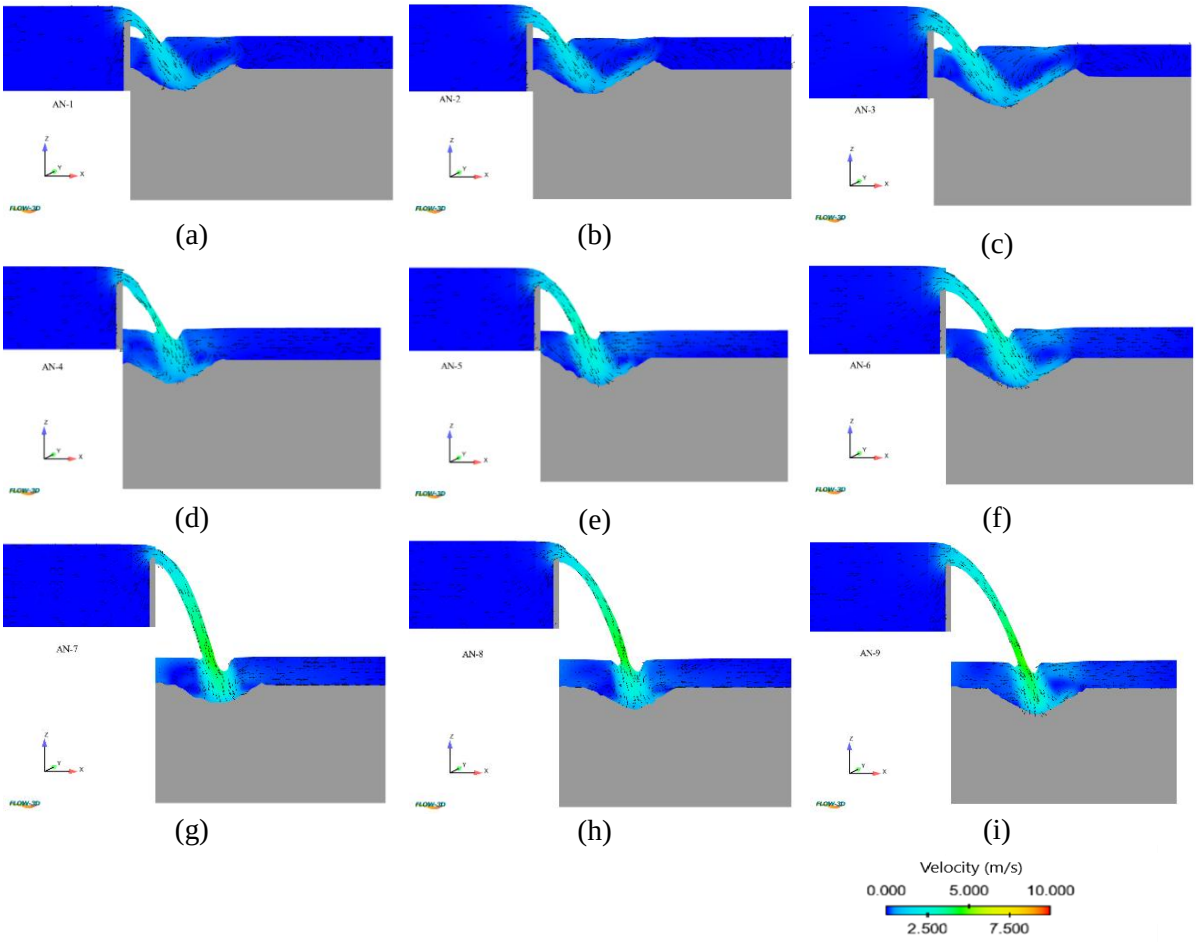

Figure 9. 2D simulation output for velocity vectors in rectangular weirs: a) AN1, b) AN2, c) AN3, d) AN4, e) AN5, f) AN6, g) AN7, h) AN8, and i) AN9

Table 4. Jet impact velocity and angle of classical contracted rectangular weir with CFD

Model No	V_x (m/s)	V_z (m/s)	V_j (m/s)	Jet Impact Angle (ζ) (º)
AN1	1.13	1.70	2.04	62.65
AN2	1.32	1.74	2.18	58.68
AN3	1.35	2.03	2.44	62.64
AN4	1.24	2.36	2.67	69.20
AN5	1.33	2.83	3.13	72.03
AN6	1.53	2.83	3.22	68.45
AN7	1.22	4.28	4.45	82.32
AN8	1.35	4.04	4.26	79.47
AN9	1.56	4.63	4.89	79.31

The parameters in figure 9 are presented in Table 5 for the contracted rectangular weir. Based on Table 5, there was an increase in the scour depth and x_1, x_2, x_3, x_m, x_b values due to the increased unit discharge for the stationary drop height and tailwater. Due to the increased discharge in 0.25 m and 0.50 m drop heights, it was observed that the upstream and downstream slope angles generally increased as well. However, due to the increased discharge in a 1.00 m drop height, the upstream slope angle increased while the downstream slope angle decreased. This situation may be attributed to the highly turbulent

nature of the submerged jet was highly turbulent, and a complex three-phase turbulent flow occurred with the increasing unit discharge and drop height (Fig. 9).

Table 5. Scour depth parameters

Model No	x_1 (m)	x_2 (m)	x_m (m)	x_3 (m)	x_b (m)	d_s (m)	Δx (m)
AN1	0.365	0.34	0.365	0.400	0.770	0.165	0.076
AN2	0.394	0.371	0.453	0.490	0.940	0.185	0.080
AN3	0.431	0.474	0.536	0.570	1.110	0.216	0.094
AN4	0.383	0.345	0.383	0.380	0.760	0.182	0.040
AN5	0.498	0.395	0.498	0.400	0.890	0.212	0.020
AN6	0.492	0.445	0.592	0.480	1.070	0.242	0.040
AN7	0.486	0.273	0.620	0.310	0.930	0.160	0.050
AN8	0.416	0.260	0.600	0.370	1.060	0.178	0.033
AN9	0.426	0.430	0.780	0.450	1.230	0.231	0.040

The variations that rely on time in the scour depth of the contracted rectangular weir section using CFD are presented in Figure 10. Since the water jet impact velocity and angle were low for low unit discharges and low drop heights, the maximum scour point was closer to the hydraulic structure. However, the maximum scour depth was observed to be more distant from the hydraulic structure due to the increase in the momentum force. The proximity of the scour pit to the hydraulic structure led to an increase in the apron length. The review of AN-1, AN-2 and AN-3 analysis findings revealed that while the maximum scours for low flow rate occur around 0.40 m distance from the weir, this value to 0.60 m as the unit flow rate increased. The analysis of AN-1, AN-4, and AN-7 revealed that the distance between the weir and the point of the maximum scour increased with the increased head height.

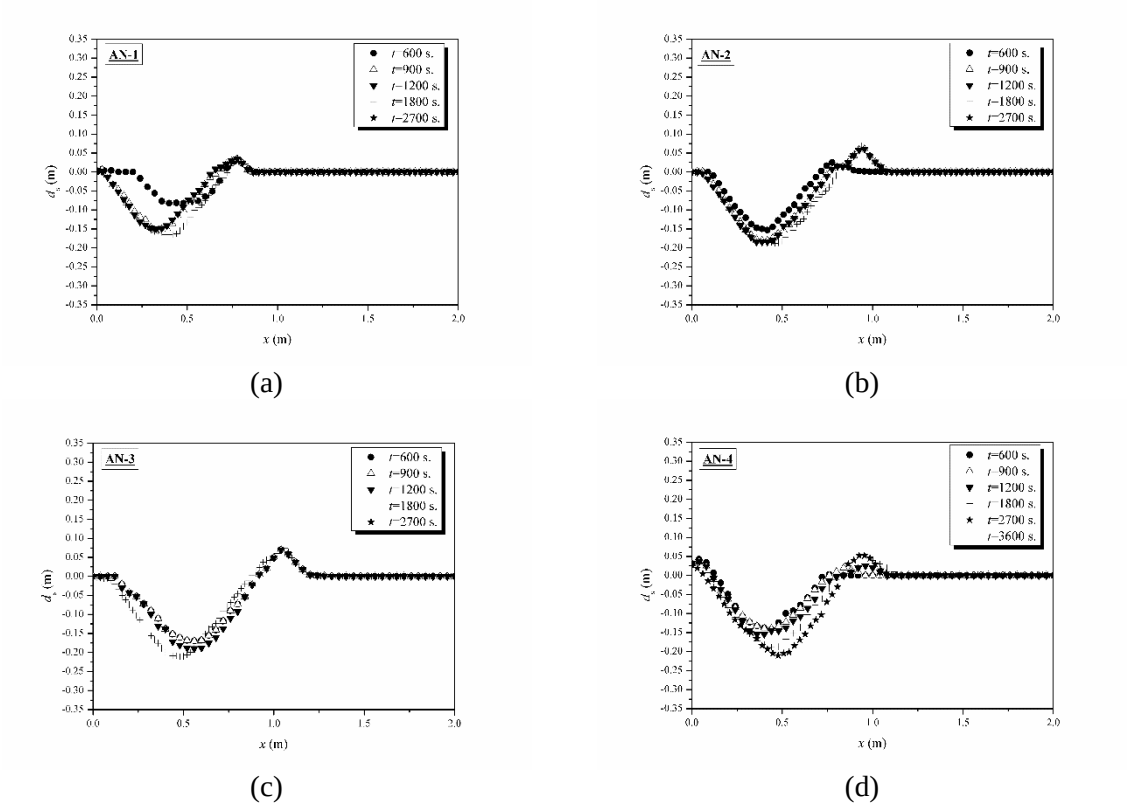

Figure 10. Scour depth longitudinal section vs time for: a) AN1, b) AN2, c) AN3, d) AN4, e) AN5, f) AN6, g) AN7, h) AN8, i) AN9

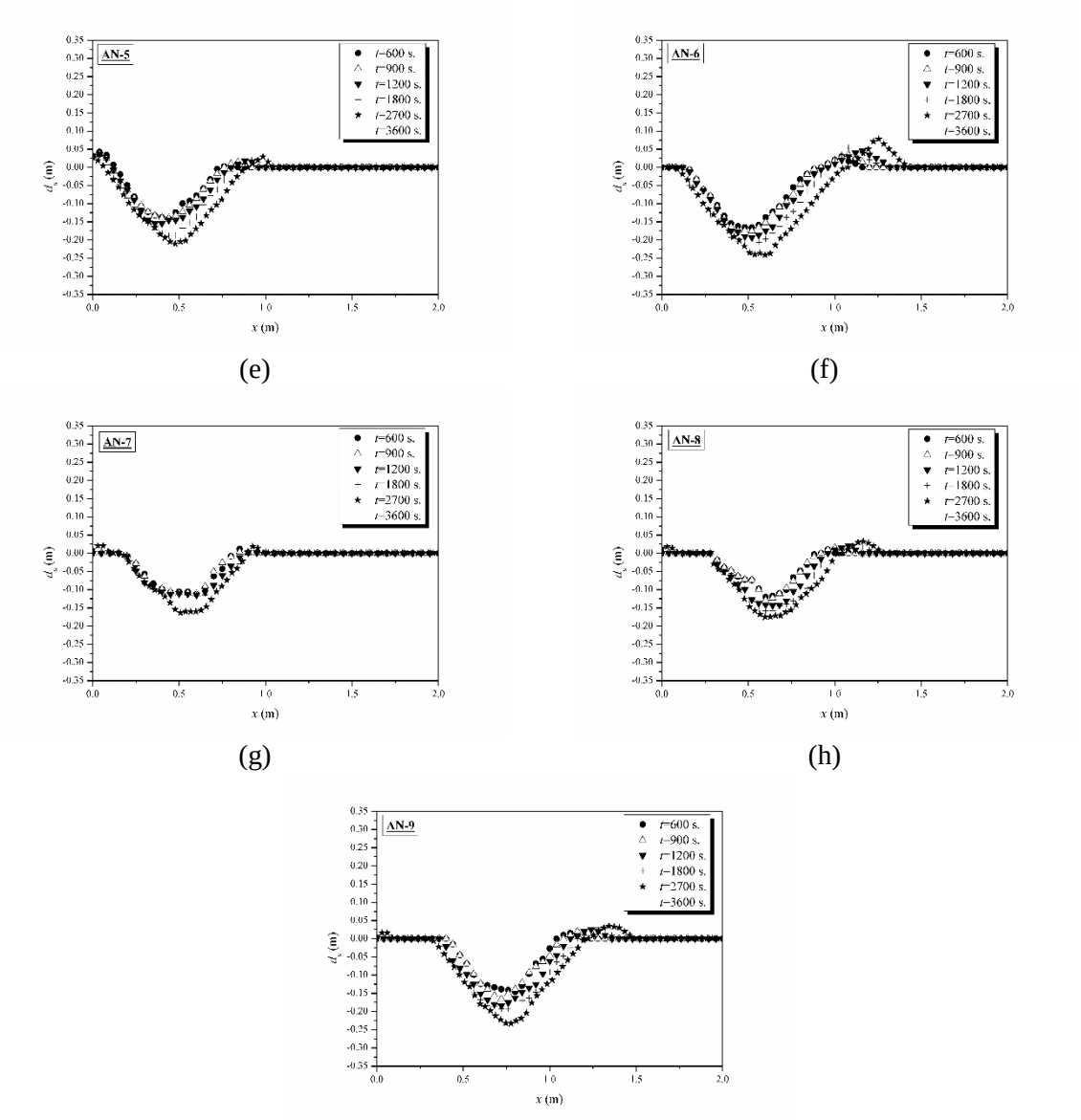

Figure 10. (Continue) Scour depth longitudinal section vs time for: a) AN1, b) AN2, c) AN3, d) AN4, e) AN5, f) AN6, g) AN7, h) AN8, i) AN9

Several researchers conducted experimental studies and reported equations for the equilibrium depth for free-overfall weirs. Veronese [38] reported one of the first findings and suggested that in several experimental studies conducted by decreasing grain diameter, the scour depth for sediments smaller than 5 mm was independent of the sediment size. The researcher suggested Eq. (13) to predict the equilibrium scour depth.

$$d = 1.90H^{0.225}q^{0.54} - h_t \tag{13}$$

Chian [39] proposed Eq. (14) for the scour depth at spillway downstream.

$$d = 1.18H^{0.235}q^{0.51} - h_t \tag{14}$$

Figure 11 compares the present study results with empirical equations using Eqs. (13-14). Comparing the findings with various unit discharge and drop heights revealed that the results obtained from the

proposed equations by Veronese [38] and Chian [39] were quite different. Therefore, several parameters affect the scouring event, which could be the reason for this difference.

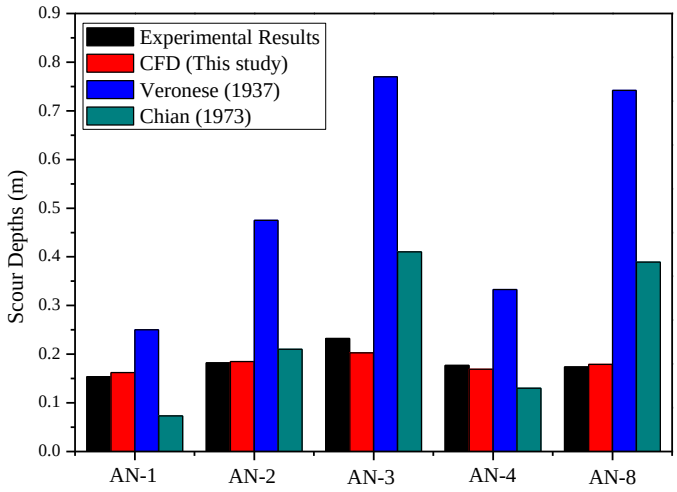

Figure 11. Comparison of scour depths using empirical equations

4. Conclusions

This study provides both theoretical and practical implications for local scour downstream of contracted rectangular weirs under free overfall conditions. The CFD results clarify how unit discharge and drop height control the time development and magnitude of scour, the variation of jet impact velocity and angle, together with the location of maximum scour for contracted weir geometries that are widely used in hydraulic engineering practice. From an engineering perspective, the obtained relationships can be used to estimate required apron length and protection thickness, to position and design scour protection and plunge pools more effectively. The significant findings obtained from this study are highlighted below.

- Approximately 90% of the equilibrium scour depth occurred within the first 15 minutes, which is consistent with the literature.
- The scour depth increases significantly with increasing unit discharge and the drop height.
- It was found that the air bubbles entering with the plunging jet have a decreasing effect on the scour depth, which is consistent with the literature.
- In addition, the numerical results agree with the experimental results. The numerical models in this aspect can be a helpful tool to investigate complicated multi-phase flows, such as scour problems, as well as other turbulent flows, when calibrated with some experimental data.
- The numerical simulations were calibrated and validated against experiments conducted with a single sediment type, a fixed tailwater depth, and a specific contracted rectangular weir geometry. These situations are limitations of this study.
- Future research should extend the CFD-based framework to graded sediments, variable tailwater conditions, and different weir configurations.

5. Acknowledgments

This research is based on Erdinc Ikinciogullari's PhD dissertation [40]. The TUBITAK MAG115M478 project [30], in which Erdinc Ikinciogullari participated as a scholarship student, provided the Flow-3D software utilized in this work. For its contributions, we acknowledge TUBITAK. We also acknowledge Dr Mustafa TUNC for his contributions to the experimental data.

6. Author Contribution Statement

Author 1, a doctoral student, conducted the literature review and numerical simulations, and assisted in the interpretation of the results. Author 2 served as the supervisor and provided guidance on the interpretation of findings. Author 3, as the co-supervisor, contributed to the numerical aspects of the study.

7. Ethical Statement Regarding the Use of Artificial Intelligence

This study was not prepared using any artificial intelligence-based technologies or software. The author prepared all the study's content in compliance with academic ethical standards and scientific research methodologies. During the preparation of this work, the authors used the Grammarly and Gemini Pro applications to improve language and readability.

8. Ethics Committee Approval and Conflict of Interest

“There is no conflict of interest with any person/institution in the prepared article. Additionally, ethics committee approval is not required for this study.”

9. References

[1] O. R. Stein and P. Y. Julien, "Sediment concentration below free overfall," *J. Hydraul. Eng.*, vol. 120, no. 9, pp. 1043–1059, 1994.
[2] M. Ghodsian, B. Melville and D. Tajkarimi, "Local scour due to free overfall jet," *Proc. Inst. Civ. Eng. Water Manag.*, vol. 159, no. 4, pp. 253–260, 2006.
[3] S. Dey and R. V. Raikar, "Scour below a high vertical drop," *J. Hydraul. Eng.*, vol. 133, no. 5, pp. 564–568, 2007.
[4] M. Ghodsian, M. Mehraein and H. R. Ranjbar, "Local scour due to free fall jets in non-uniform sediment," *Sci. Iran.*, vol. 19, pp. 1437–1444, 2012.
[5] N. R. B. Olsen and M. C. Melaaen, "Three-dimensional calculation of scour around cylinders," *J. Hydraul. Eng.*, vol. 119, no. 9, pp. 1048–1054, 1993.
[6] B. Lin and R. A. Falconer, "Numerical modelling of three-dimensional suspended sediment for estuarine and coastal waters," *J. Hydraul. Res.*, vol. 34, no. 4, pp. 435–456, 1996.
[7] J. E. Richardson and V. G. Panchang, "Three-dimensional simulation of scour-inducing flow at bridge piers," *J. Hydraul. Eng.*, vol. 124, no. 5, pp. 530–540, 1998.
[8] W. Wu, W. Rodi and T. Wenka, "3D numerical modeling of flow and sediment transport in open channels," *J. Hydraul. Eng.*, vol. 126, no. 1, pp. 4–15, 2000.
[9] B. Y. Jia, T. Kitamura and S. S. Y. Wang, "Simulation of scour process in plunging pool of loose bed-material," *J. Hydraul. Eng.*, vol. 127, no. 3, pp. 219–229, 2001.
[10] X. Liu and M. H. García, "Three-dimensional numerical model with free water surface and mesh deformation for local sediment scour," *J. Waterw. Port Coastal Ocean Eng.*, vol. 134, no. 4, pp. 203–217, 2008.
[11] J. A. Vasquez and B. W. Walsh, "CFD simulation of local scour in complex piers under tidal flow," in *Proc. 33rd IAHR Congr., Int. Assoc. Hydraul. Eng. Res.*, 2009.
[12] S. Abbasi, A. Kamanbedast and J. Ahadian, "Numerical investigation of angle and geometric of L-shape groin on the flow and erosion regime at river bends," *World Appl. Sci. J.*, vol. 15, no. 2, pp. 279–284, 2011.
[13] L. G. Castillo and J. M. Carrillo, "Scour estimation of the Paute-Cardenillo Dam," in *Proc. Int. Perspect. Water Resour. Environ.*, Quito, Ecuador, 2014, pp. 8–10.
[14] G. Epely-Chauvin, G. De Cesare and S. Schwindt, "Numerical modelling of plunge pool scour evolution in non-cohesive sediments," *Eng. Appl. Comput. Fluid Mech.*, vol. 8, no. 4, pp. 477–487, 2014.
[15] M. C. Aydin and E. Isik, "Using CFD in hydraulic structures," *Int. J. Sci. Technol. Res.*, vol. 1, no. 5, pp. 7–13, 2015.
[16] A. L. J. Pang, M. Skote, S. Y. Lim, J. Gullman-Strand and N. Morgan, "A numerical approach for determining equilibrium scour depth around a mono-pile due to steady currents," *Appl. Ocean Res.*, vol. 57, pp. 114–124, 2016.
[17] H. Pourshahbaz, S. Abbasi and P. Taghvaei, "Numerical scour modeling around parallel spur dikes in FLOW-3D," 2017.
[18] C. Man *et al*., "Assessment of turbulence models on bridge-pier scour using Flow-3D," *World J. Eng. Technol.*, vol. 2, no. 2, pp. 241–255, 2019.
[19] M. C. Aydin, M. E. Emiroglu, A. E. Ulu and E. Ikinciogullari, "Investigation of local scours under vertical drop using CFD," *Düzce Univ. J. Sci. Technol.*, vol. 10, no. 1, pp. 239–248, 2019.
[20] E. Ikinciogullari, M. E. Emiroglu and M. C. Aydin, "Comparison of scour properties of classical and trapezoidal labyrinth weirs," *Arab. J. Sci. Eng.*, vol. 47, pp. 4023–4040, 2022.
[21] L. Kumar and M. S. Afzal, "Computational fluid dynamics modeling of scour around abutment geometries under combined effects of waves and currents," *Ocean Eng.*, vol. 294, p. 116812, 2024.
[22] X. Wang, W. Li, Z. Peng, Q. Yu, Y. Yang and J. Li, "Optimization of combined scour protection for bridge piers using computational fluid dynamics," *Water*, vol. 17, p. 2742, 2025.
[23] M. C. Aydın and Ç. Karaduman, "Kapak altı batmış akım mansabında meydana gelen oyulmaların sayısal simülasyonu," *Pamukkale Univ. J. Eng. Sci.*, vol. 24, no. 3, pp. 439–443, 2018.
[24] S. Dey and A. Sarkar, "Characteristics of submerged jets in evolving scour hole downstream of an apron," *J. Eng. Mech.*, vol. 134, no. 11, pp. 927–936, 2008.

[25] X. Yan, A. Mohammadian and C. D. Rennie, "Numerical modeling of local scour due to submerged wall jets using a strict vertex-based, terrain conformal, moving-mesh technique in OpenFOAM," *Int. J. Sediment Res.*, vol. 35, pp. 237–248, 2020.
[26] B. D. Adhikary, A. P. Majumdar and M. Kostic, "CFD simulation of open channel flooding flows and scouring around bridge structures," in *Proc. 6th WSEAS Int. Conf. Fluid Mech.*, 2009.
[27] M. Zhao, L. Cheng and Z. Zang, "Experimental and numerical investigation of local scour around a submerged vertical circular cylinder in steady currents," *Coast. Eng.*, vol. 57, pp. 709–721, 2010.
[28] Z. W. Zhu and Z. Q. Liu, "CFD prediction of local scour hole around bridge piers," *J. Cent. South Univ. Technol.*, vol. 19, pp. 273–281, 2012.
[29] W. Xiong, P. Tang, B. Kong and C. S. Cai, "Computational simulation of live-bed bridge scour considering suspended sediment loads," *J. Comput. Civ. Eng.*, vol. 31, p. 04017040, 2017.
[30] TÜBİTAK, *115M478 – Serbest düşülü savakların mansabında oluşan yerel oyulmanın deneysel ve sayısal araştırılması*, Project Report, 2019.
[31] R. L. Soulsby and R. J. S. Whitehouse, "Threshold of sediment motion in coastal environments," in *Proc. Pacific Coasts Ports '97*, 1997.
[32] D. R. Mastbergen and J. H. Van den Berg, "Breaching in fine sands and the generation of sustained turbidity currents in submarine canyons," *Sedimentology*, vol. 50, pp. 625–637, 2003.
[33] E. Meyer-Peter and R. Müller, "Formulas for bed-load transport," in *Proc. 2nd Meet. Int. Assoc. Hydraul. Struct. Res.*, Stockholm, 1948.
[34] Flow Science, *Sediment Scour Model, FLOW-3D User Manual, Version 11.0.3*. Santa Fe, NM, USA: Flow Science, Inc., 2014.
[35] F. Fan, B. Liang, Y. Bai, Z. Zhu and Y. Zhu, "Numerical modeling of local scour around hydraulic structure in sandy beds by dynamic mesh method," *J. Ocean Univ. China*, vol. 16, pp. 738–746, 2017.
[36] S. Liu, Y. Yang and X. Wu, "Simulations of local scour around a cylindrical bridge pier and a semicircular abutment using unsteady k–ε model combined with σ-grid," *Open Civ. Eng. J.*, vol. 11, pp. 598–614, 2017.
[37] A. Baylar and M. E. Emiroglu, "The role of weir types in entrainment of air bubbles," *Int. J. Sci. Technol.*, vol. 2, no. 2, pp. 143–154, 2007.
[38] A. Veronese, *Erosion de fond en aval d'une décharge*. Soc. Coop. Tipogr., 1937.
[39] M. W. Chian, "Scour at downstream end of dams in Taiwan," in *Proc. IAHR Int. Symp. River Mech.*, Bangkok, 1973.
[40] E. Ikinciogullari, "Serbest düşülü savakların mansabında oluşan yerel oyulmanın sayısal analizi," Ph.D. dissertation, Inst. Sci., Fırat Univ., Elazığ, Turkey, 2019.